Electronic properties of α-quartz under high pressure and the transition to the amorphous phase

A. Di Pomponio and A. Continenza
Dipartimento di Fisica, Università degli studi de L'Aquila, Coppito - L'Aquila, I-67010, Italy
(Received 23 February 1994)

The electronic properties of α-quartz, at ambient pressure and in connection with the structural deformation induced by compression, are examined via first-principles calculations, based on the full-potential linearized augmented-plane-wave method. A detailed analysis of the density of states and of the charge density as a function of pressure is presented. The results at ambient pressure are in good agreement with experiments and earlier theoretical studies. We found that the forbidden energy range between Si-O bonding and O $2p$ nonbonding states vanishes in the region of the transition to the amorphous phase, indicating a strong hybridization between these states. This hybridization turns out to be more compatible with a different Si coordination and may lead, by local rearrangement, to the formation of a mixed phase. The fundamental band gap is found to increase with pressure.

I. INTRODUCTION

The interest in silica as a material soughtful for technological application in electronic devices is growing steadily. Quartz-controlled oscillators have been widely used in timing devices and in sophisticated signal filters, because of their excellent stability. Moreover, in modern semiconductor technology, SiO_2 films grown on pure silicon have been employed in the construction of integrated circuits and in various devices (e.g., metal-oxide–semiconductor field-effect transistors).

On the other hand, the interest in silicon dioxide is not merely confined to the material science and technology. Silicon dioxide constitutes, in fact, an important component of the Earth's mantle: The polymorphs coesite and stishovite are present with magnesium silicates (especially Mg_2SiO_4 and $MgSiO_3$) and aluminum silicates (garnet-type structures), as inferred by many reliable models and confirmed by experimental investigations.

Nevertheless, silica is not a very simple and straightforward material to study; it exists in many and various allotropic forms.[1] The most common ones, including α-quartz, are built from the same fundamental structural unit: the SiO_4 tetrahedron. In this arrangement, each silicon is bound to four oxygen atoms and each oxygen to two silicon atoms. The Si-O-Si angle varies from one polytype to another and the overall symmetry of the system is determined on the way all the tetrahedra are linked together.

The electronic properties of SiO_2 have been investigated quite extensively over the past years. Many experimental studies have been performed by means of optical method,[2–4] x-ray emission,[5,6] and ultraviolet and x-ray photoelectron spectroscopy.[7–9]

α-quartz is the stable form of SiO_2 at room temperature and at pressures lower than 3 GPa. At higher pressures, α-quartz persists as a metastable structure and undergoes a gradual transition to the amorphous phase approximately in the range 15–30 GPa. The experimental evidence of this order-disorder transformation in some polymorphs of silica has been established by means of x-ray diffraction measurements both on powdered samples[10] and on single crystals,[11] and confirmed by more recent high-resolution transmission electron microscopy (HRTEM) measurements.[12] Such a direct crystalline-to-amorphous transition, observed in a number of oxides,[13,14] is of fundamental interest since characteristic properties are exhibited by disordered solids, like the so-called "memory effect."[14,15] In particular, it has been observed that the amorphization of silica is irreversible: After pressure release, it remains an anisotropic material, conserving only partial memory of the crystalline structure.[15]

Most of the theoretical work has attempted to interpret the experimental observations in terms of semiempirical models.[16–18] In addition, many first-principles calculations have been carried out on molecular clusters of various sizes,[19–21] with the aim to simulate the main structural building units of silica polymorphs and to understand their bonding properties. Frequently, classical force fields have been derived from these quantum mechanical studies and used in molecular dynamics simulations of the structural phase transition[20,22–24] and in the calculation of vibrational modes.[25]

Because of the relatively complex structures of all the polytypes, there have been few *ab initio* solid-state calculations of the electronic properties of silicon dioxide:[26–29] almost all of them restricted to the equilibrium structure. Recently, an all-electron investigation of the new ultrahigh-pressure phase of silica[30] has appeared. Up to now, only one first-principles study,[31] based on the pseudopotential plane-wave approach, has appeared regarding the pressure effects on the structural and electronic properties.

0163-1829/94/50(9)/5950(7)/$06.00 ©1994 The American Physical Society

In this paper, we present an all-electron study of the electronic properties of α-quartz under pressure, near and above the region of the amorphous transition. The structural properties related to the modification of α-quartz upon compression have been discussed in a previous paper.[32] There, it was shown that pressure induces an enormous reduction of the structural voids which, in turn, causes a rapid decrease of the intertetrahedral Si-O-Si angles and O-O distances. In the range 15–30 GPa, the presumed pressure range for the order-disorder transition, these related parameters fall below the smallest value experimentally observed in all crystalline silicates. We were able to observe that the large increase of the strain energy associated with this deformation can be the cause of the transition to the amorphous state. Moreover, we found that at the maximum compression considered (~56 GPa), the configurational parameters match very closely the corresponding values of the ideal structure proposed by Sowa[33] for the high-pressure phase: The oxygen anions are found to approach a close-packed configuration.

The main aim of the present paper is to analyze the electronic structure of α-quartz in the region of the order-disorder transition; since electronic and structural properties are intimately connected, new insights on the microscopic mechanism of the transformation can be obtained. The electronic behavior at very high pressure, far above the transition region, is also discussed: The trends observed in limit conditions improve the understanding of the structural changes.

II. COMPUTATIONAL DETAILS

The theoretical description of α-quartz is difficult since its structure is quite complicated and the nature of the electronic interactions in this material rather complex. The unit cell is very large and contains six oxygen and three silicon atoms. The symmetry is quite low (D_3^6 space group, six symmetry operations only) and the structure is defined by four fractional coordinates and two lattice parameters.

The electronic properties have been analyzed for different volume values V of the unit cell, corresponding to pressures ranging from about -3 to 56 GPa.[32] For each fixed value of the volume V, we minimized the total energy of the system with respect to all the free configurational parameters. The equilibrium structural parameters obtained as a function of pressure are reported in Ref. 32.

The calculations have been carried out within the local-density approximation (LDA) to the density functional theory, as parametrized by Hedin and Lundqvist,[34] using the full-potential linearized augmented-plane-wave (FLAPW) method.[35] The technique of special $\mathbf{k}$ points[36] has been used for the $\mathbf{K}$-space integration (we considered three special $\mathbf{k}$ points). Self-consistency was achieved using a cutoff $R_{\mathrm{max}}K_{\mathrm{max}} = 6$ which, at the equilibrium experimental structure, results in about 830 LAPW basis functions. The charge density in the muffin-tin spheres was determined using a radial mesh of 321 points, with a logarithmic step of 0.035. The O $2s$ and $2p$ states as well as the Si $3s$ and $3p$ states were treated variationally as valence states. For an accurate description of the electronic density of states (DOS), the Hamiltonian was diagonalized at 60 $\mathbf{k}$ points in the irreducible part of the hexagonal Brillouin zone within the linear tetrahedron method.[37]

III. RESULTS AND DISCUSSION

A. Electronic properties at room pressure

The calculated density of states (DOS) of α-quartz at room pressure is reported in Fig. 1 (solid line) and compared to results from x-ray photoemission spectroscopy (XPS) (dashed line) given in Ref. 9. In the valence band we can observe the presence of three main groups of peaks well separated in energy. These features can be related to the following states: oxygen $2s$ semicore localized states (the lowest and isolated peaks, label A in Fig. 1), oxygen $2p$ silicon ($3s$, $3p$) bonding states (intermediate region, label B), and oxygen $2p$ nonbonding states (upper peaks, label C).

The lowest part of the valence band (A), from -19.5 to approximately -17.0 eV, is mainly made of O $2s$ states. This is clear by inspection of Fig. 2, where the projected densities of states (PDOS) per atomic and per each angular momentum component are reported. In particular, from Fig. 2(d) we can note a quite small contribution from Si s and p states; nevertheless, the dominant O $2s$ component determines the extension and the overall shape of the DOS in this region. The calculated energy position of the O $2s$ states is higher than experiment by approximately 2 eV: The XPS O $2s$ peak is located at ~20.5 eV below the valence band maximum (VBM), while the calculated peak is only ~18.5 eV below the va-

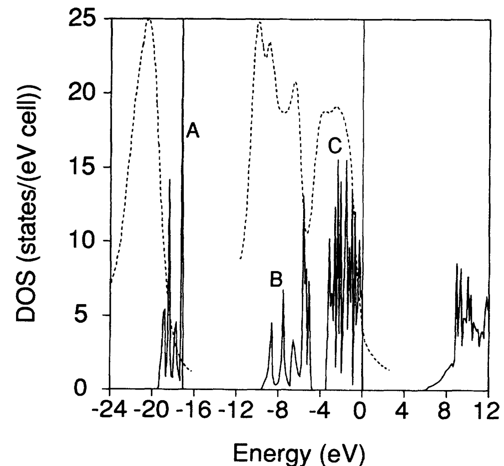

FIG. 1. Calculated density of states (solid line) of α-quartz at room pressure and XPS spectrum (dashed line) from Ref. 9. The valence band maximum is taken as the zero of the energy scale. The intensity of the XPS data is in arbitrary units.

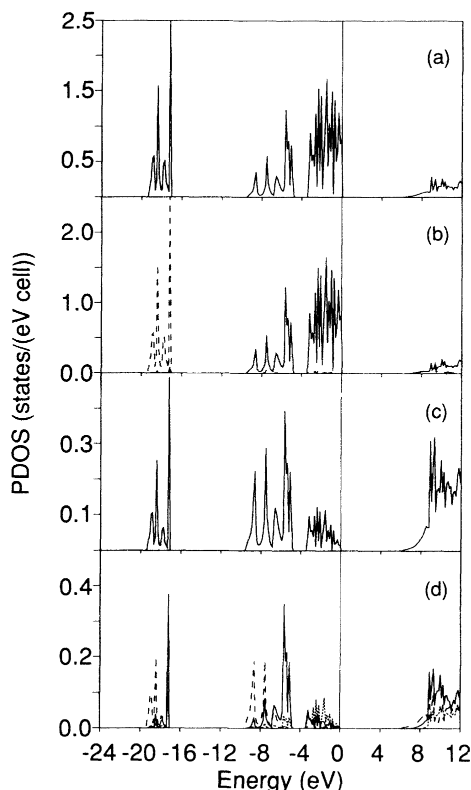

FIG. 2. Projected density of states (PDOS) of α-quartz at room pressure. Total O contribution [panel (a)]; O s (long dashed line) and p (solid line) (b); total Si contribution (c); Si s (long dashed line), p (solid line), and d (short dashed line) [panel (d)].

lence band edge. This discrepancy in the binding energy, about 10%, is related to the local-density approximation and the underestimate of the exchange-correlation energy for confined atomiclike states.

The region from about -9.6 to -5.0 eV (B) consists of O-Si bonding orbitals. The main component is represented by oxygen p states, which determine the extension and the global shape of these peaks. The bottom edge of this DOS region is somewhat higher than experiment (about 2.1 eV). In agreement with photoemission measurements, we can distinguish three main structures corresponding to different contribution from silicon and oxygen states, as can be seen from Fig. 2. The O p states contribute to all these fine structures, while Si s states contribute to the lowest peaks (located between -9.0 and -7.5 eV) and Si p states to the upper peaks (at -6.0 eV).

The highest part of the valence band (C, from about -3.5 eV up to the top of the valence band, taken as the zero of the energy scale) is prevalently composed by oxygen p nonbonding orbitals (see discussion below), with a quite small contribution from Si p and d states, as shown in Fig. 2. The theoretical DOS exhibits many fine structures, while the experimental spectrum shows only one main peak and some minor features. It is interesting to note that these fine structures are completely absent on UV and x-ray photoelectron spectra of amorphous silica:[7] Therefore they can be associated with the long-range order of the crystal, as confirmed also by tight-binding calculations[18] on α-quartz and on the SiO_2 Bethe lattice.

We note that the contribution due to the oxygen d states is lacking in the range of energy examined. In addition, there is no mixing between oxygen s and p states, while the contribution due to silicon s, p, and d states is spread fairly uniformly all over the valence band.

The lowest empty states of the DOS have substantially O s-p and Si s-p character; in particular, the bottom of the conduction band is determined prevalently by O and Si s states (Fig. 2). Its fairly abrupt onset is found also by Chelikowsky *et al.*[31] in a previous theoretical study, within a pseudopotential plane-wave approach. There is a general and excellent agreement with their results, in particular, as regard to the widths and positions of the DOS peaks.

The comparison of our results with earlier calculations gives also a satisfactory agreement. The results obtained by Xu and Ching[29] from self-consistent OLCAO (orthogonalized linear combinations of atomic orbitals) calculations, within LDA, are in good quantitative agreement with our findings. The valence DOS of α-quartz determined by Laughlin *et al.*,[18] using an empirical tight-binding Hamiltonian, shows an analogous composition, although the width of the highest part of the valence band is $\sim$1.5 eV larger than our value. Moreover, the mean position of the lowest isolated DOS peaks is about 2 eV lower than what was predicted by our calculations. Some differences exist also with previous Hartree-Fock results:[27] a smaller separation is obtained between the highest and the intermediate valence DOS peaks (labels B and C in Fig. 1) and the mean position of O $2s$ peaks (A in Fig. 1) is lower of about 5 eV. The mean binding energy of these peaks is even larger ($\sim$3 eV) than the XPS O $2s$ peak, due to the Hartree-Fock approximation which disregards correlation effects. In addition, the width of the intermediate peak in the valence band is about 2 eV larger than our case. Nevertheless, both our and their results agree within 1 eV with XPS data. On the other hand, the orbital decomposition of the valence band states is in good agreement with our findings.

α-quartz is an insulator, with an indirect gap. At room pressure, we find that a 5.75 eV band gap occurs between the VBM at K and the bottom of the conduction band at Γ. The extremum of the valence band at M is slightly lower ($\sim$0.04 eV) than the value at K, while at the other high-symmetry points of the Brillouin zone the VBM is a few tenths of eV lower than at K (e.g., the top of the valence band at Γ is 0.35 eV lower). We find an excellent agreement with previous calculations[31] as far as the value of the band gap is concerned and its indirect nature K_v-Γ_c.

As expected from LDA calculations, the theoretical band gap underestimates the real optical gap (about 8.9 eV),[4] measured via photoconductivity experiments on amorphous silica; nevertheless, the similarity between experimental spectra[2,3,7,9] and theoretical calculations of amorphous SiO_2 and crystalline α-quartz[18] indicates that the overall electronic structure in the ordered phase

should be very similar to what it is in the amorphous state.

In Fig. 3 we show the valence charge density, projected on the Si-O-Si bonding plane. It is possible to observe that most of the electron charge density is localized in the interatomic region between Si and O, corresponding to the formation of the bond, mainly due to the p states of silicon and oxygen, as already pointed out. The charge accumulation localized at the oxygen site, pointing away from silicon, corresponds to O p-like nonbonding states.

We can notice that a charge transfer takes place when the interatomic bonds are formed. This is highlighted by the electronic charge deformation map, i.e., the difference between the crystal charge density and the superposition of the atomic charge densities, displayed in Fig. 3(b). The observed charge accumulation at the oxygen site comes from regions close to the silicon atoms, prevalently away from the Si-O bonding directions.

Let us look now at how the three main groups of valence states, well separated in energy, contribute to the charge density. In the three panels of Fig. 4, we show these different contributions on the plane cutting the Si-O-Si angle. In Figs. 4(a), (b), and (c) we plotted the electronic charge density corresponding to the lowest states (label A in Fig. 1), the intermediate states (B), and the highest region (C) of the valence band, respectively. We would like to point out the different shapes of the charge density in these plots: the typical spherical shape of the charge density coming from O $2s$ states [Fig. 4(a)], the bonding nature of the O p-like orbitals, oriented along the Si-O direction [Fig. 4(b)], and, finally, the nonbonding character of oxygen p orbitals [Fig. 4(c)], well localized on the atomic site and oriented transversally with respect to the bonding direction.

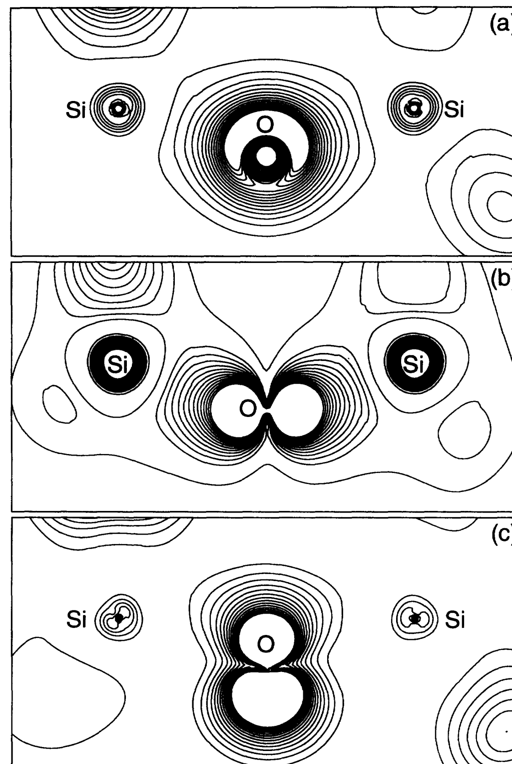

FIG. 4. Charge density corresponding to the lowest valence states [panel (a)] (-19.5 to -17.0 eV, label A, Fig. 1), to the intermediate valence states [panel (b)] (-9.5 to -5.0 eV, label B, Fig. 1), and to the highest valence states [panel (c)] (-3.5–0.0 eV, label C, Fig. 1) at room pressure. Charge densities are projected in the Si-O-Si bonding plane. Lines of equal value are separated by $10e$/(unit cell volume).

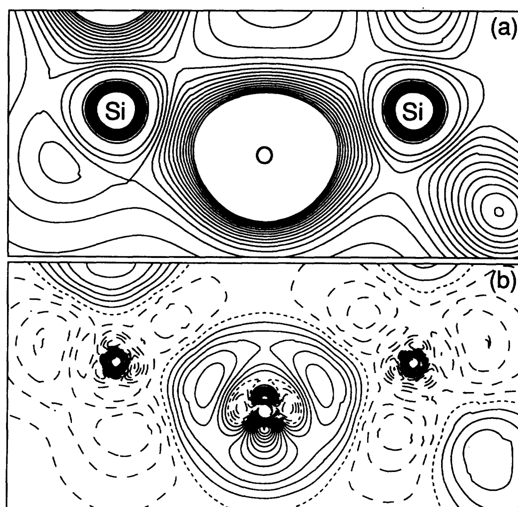

FIG. 3. Valence charge density (a) and difference between the crystal charge density and the superposition of atomic charge densities (b) at room pressure, projected in the Si-O-Si bonding plane. Lines of equal value are separated by $10e$/(unit cell volume) and $5e$/(unit cell volume) in panels (a) and (b), respectively. In panel (b), long dashed, short dashed, and solid lines corresponds to differential charge density negative, zero, and positive, respectively.

B. Pressure effects on the electronic structure

The analysis of the pressure-induced changes in the electronic structure of α-quartz allows a deeper understanding of the structural modifications of the crystal. In particular, we examine here the electronic properties in the region of the amorphous transition (15–30 GPa) and in the limit case considered, i.e., for a compression $V/V_{eq} = 0.655$ (V_{eq} being the unit cell volume at ambient pressure) corresponding to about 56 GPa.[32] This case is of interest since the structure at this pressure reproduces the Sowa's model[33] with the oxygen atoms arranged in a close-packed configuration. The most interesting modifications of the electronic properties are observed upon high compression; in fact, under moderate hydrostatic pressure (up to ∼6 GPa), the changes of the electronic structure are not so relevant and reflect the fair linearity of the structural deformations.[32]

In Figs. 5(a) and (b) the calculated total DOS at intermediate (∼30 GPa) and at maximum (∼56 GPa) com-

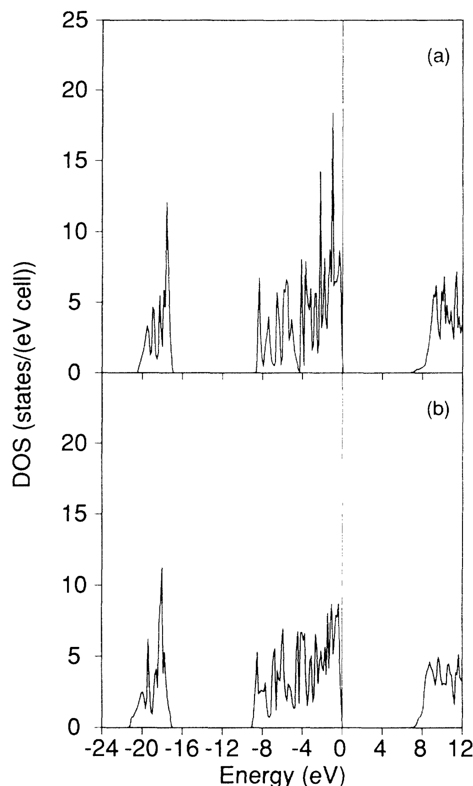

FIG. 5. Calculated density of states for α-quartz at intermediate (~30 GPa) (a) and maximum (~56 GPa) (b) compression.

pression, respectively, are displayed. The main and striking change in Fig. 5(b) with respect to the DOS at ambient pressure (Fig. 1, solid line) is the vanishing of the forbidden energy region (centered at about −4.0 eV) between the B and C peaks. As is clearly seen in Fig. 5(a), the closing of this gap (between bonding and nonbonding states) starts at about 30 GPa. This effect is due to the hybridization between the O $2p$ Si bonding states and the O $2p$ nonbonding states. We note that the main features of the intermediate DOS peaks at 30 GPa are preserved and that the different contribution from silicon s and p states is still responsible for the three main structures present in this region. The partial closing of the gap is caused by a rigid shift towards higher energy values (about 1.0 eV) of the B region together with a widening of the C region. At 56 GPa, the strong mixing of the B and C peaks in a single feature is dominated by the oxygen p states, with a small contribution from Si states. We also point out that pressure induces a modification of the shape of the lowest A peaks (O $2s$ states) causing a significant broadening and a lowering of the bottom edge (about 1.0 and 1.9 eV at 30 and 56 GPa, respectively). In addition, the contribution of the oxygen d states to the valence band disappears completely as pressure is applied. As regard to the Si states, we note a prevalent contribution from s and p states at characteristic energy values, while the d states are present fairly uniformly over the entire valence band. Another effect induced by pressure is the onset of the conduction band, determined especially by Si s and p states, which becomes increasingly abrupt.

The valence charge density in the Si-O-Si bonding plane at 56 GPa is displayed in Fig. 6(a). The large bond bending under high pressure [the Si-O-Si angle is ~116° in Fig. 6(a), while it is equal to ~144° in Fig. 3(a)] induces the main changes in the electron charge density. The overlap between the O $2p$ Si bonding states and the O $2p$ nonbonding states, already observed in the DOS, produces a more regular and spherical distribution of the electronic charge around the oxygen atom, while the partial charge accumulation on the atomic sites is, prevalently, a consequence of the homogeneous reduction of the unit cell volume.

The differential charge density displayed in Fig. 6(b) shows a change of the shape of the O nonbonding feature and a geometrically more selective charge transfer from silicon atoms to oxygen site, due to the close packing induced by pressure.

The fundamental band gap increases upon compression. Its behavior as a function of pressure is nearly linear up to ~6 GPa, as is clearly observed in Fig. 7(a). At 6.3 GPa the gap is still between K_v and Γ_c points and is found to be equal to 6.16 eV. The pressure coefficient $(\partial E_g/\partial P)_0$ at zero pressure, obtained from a fit of the linear region, is equal to 9.6 $\times 10^{-2}$ eV/GPa. At pressures above 14 GPa, the trend is highly nonlinear. The band gap is 6.37 eV at about 14 GPa, with the VBM at the M point. Therefore, the VBM switches from the K to the M point in the range 6.3–14 GPa. We point out that the difference between the top of the valence band at K and at M is a few hundredths of eV at pressures below 15 GPa. The direct gap at Γ is found to be 0.1–0.3

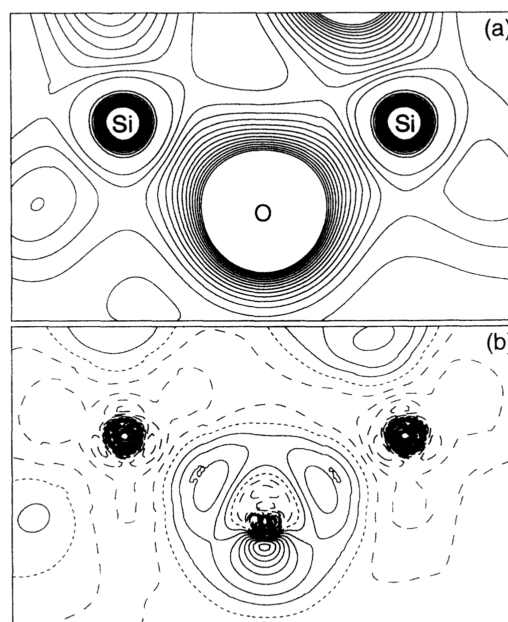

FIG. 6. Valence charge density (a) and difference between the crystal charge density and the superposition of atomic charge densities (b) at ~56 GPa, projected in the Si-O-Si bonding plane. Symbols as in Fig. 3.

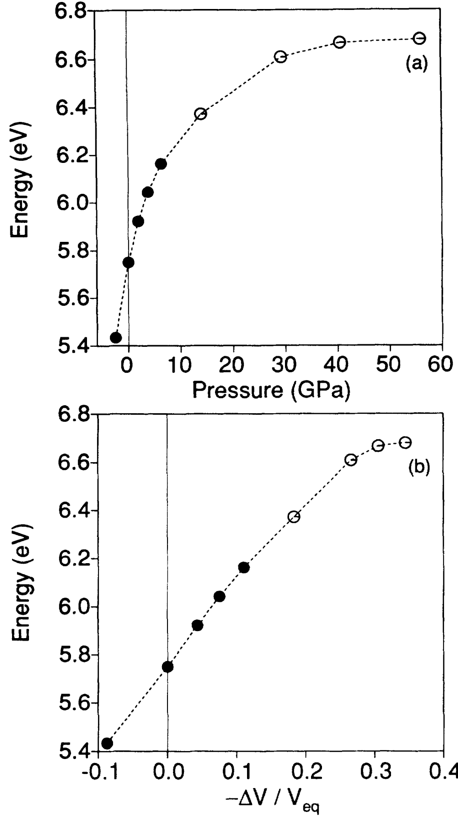

FIG. 7. Fundamental band gap as a function of pressure (a) and of the relative change in the unit cell volume $-\Delta V/V_{eq}$ (b). (•) and (∘) refer to the position of the minimum band gap: K_v-Γ_c and M_v-Γ_c, respectively.

eV larger than the minimum indirect gap, on the overall pressure range.

The displacement of the VBM from the K to the M point just described can be understood on the basis of the symmetry properties of the crystal: States corresponding to these points must be invariant under the symmetry operations at K and M, respectively. In fact, the small point group at K is made by rotations by an angle of $2\pi/3$ while at M contains π rotations around the z axis. At ambient pressure the nonbonding oxygen electrons at K and M give rise to almost pure p_z states, with minor components p_x and p_y, and yield orbitals transversal to the Si-O-Si angle. These states are of course invariant under the symmetry operations of the small point group of both K and M points. When high compression is applied, hybrid states made of oxygen p bonding and nonbonding orbitals are gradually generated, up to energies close to the VBM. These mixed states have again a dominant p_z character; nevertheless the p_x and p_y components become more and more relevant: The combinations that can be formed have the correct symmetry invariance only under the operations of the small point group of M, where the valence band maximum now occurs.

Most of the nonlinearity in the E_g-p curve disappears if the energy gap is plotted versus the relative change in the unit cell volume ($-\Delta V/V_{eq}$), as can be observed in Fig. 7(b). We can note a slightly sublinear behavior up to $-\Delta V/V_{eq} \approx 27\%$, corresponding to about 30 GPa, while it becomes nonlinear for higher values. Fitting the points in the near-linear region [Fig. 7(b), $-\Delta V/V_{eq}$ ranging from 0% to ∼27%] with a quadratic function, we obtain the following values for the coefficients $E_{g,0}$, E_0', and E_0'': $E_{g,0}$ = 5.75 eV, E_0' = 3.98 eV, and E_0'' = −2.95 eV, where $E_{g,0}$ is the gap value at equilibrium and E_0' and E_0'' represent the first and second derivatives with respect to $-\Delta V/V_{eq}$, respectively.

We should observe that most of the tetrahedral covalent solids present a nonlinear variation of the measured absorption edge as a function of pressure, while a near linearity is recovered when E_g is plotted versus the relative change of the unit cell volume (or, equivalently, the relative change of the lattice constant, in cubic crystals).[38] SiO_2 can be considered a mixed tetrahedral solid, where only some of the atoms have tetrahedrally coordinated neighbors. The behavior of the energy gap upon compression is therefore qualitatively in agreement with earlier studies on similar solid systems. Moreover, we should point out that the nonlinear variation of E_g with pressure at intermediate values (6–30 GPa) is essentially due to the nonlinear dependence of the structural parameters on pressure.[32] The onset of the nonlinear behavior at higher pressures (above 30 GPa) seems to be a feature directly related to the order-disorder transformation since it appears in the same pressure range of the transition itself.

C. Electronic properties and the transition to the amorphous phase

The hybridization between the O $2p$ Si bonding and the O $2p$ nonbonding states discussed in the preceding section can be related to the order-disorder transition.

The gradual close packing of the oxygen atoms with pressure[11,32,33] corresponds to a noticeable reduction of the distance between Si and O atoms next-nearest neighbors (e.g., at ∼30 GPa, where the onset of the hybridization effect is observed, this distance decrease of about 20% with respect to the corresponding room pressure value). A small displacement of one silicon atom can produce a change of its coordination from four to six, resulting in a mixed phase which has been also found in previous molecular dynamics simulations.[23,24] Now, we should note that the hybridization between bonding and nonbonding states has never been observed in all SiO_2 polymorphs in their range of thermodynamical stability, except that in stishovite,[27,29] the only silica polytype with Si atoms sixfold coordinated. When α-quartz is compressed at sufficiently low temperature, the crystallization to the stable high-pressure phase stishovite is kinetically inhibited. Therefore the compression gradually compacts the structure until the hybridization effects become relevant (at ∼30 GPa). At this point, a further pressure loading causes local rearrangement of the atoms, resulting in a mixed phase where Si anions are coordinated in part tetrahedrically and in part octahedrically. This mixed coordination (four and six) is found to be topologically more compatible with the hybridization process.

This could be a possible mechanism of amorphization, since it relieves the stress of the structure upon high compression and, at the same time, lowers the cost of the hybridization between O p bonding and nonbonding states.

IV. CONCLUSIONS

We presented a FLAPW study of the electronic properties of α-quartz and their dependence on hydrostatic high compression. At room pressure we obtain results in good agreement with experiments and earlier theoretical investigations. The significant changes in the electronic structure induced by pressure occur near the region of the order-disorder transition, where the nonlinear effects are prevalent. In this pressure region we observe the occurrence of many different effects: (i) The forbidden energy range between the O $2p$ Si bonding states and the O $2p$ nonbonding states starts to vanish; (ii) the fundamental band gap behavior with pressure becomes highly nonlinear; (iii) the VBM displaces from K to M; (iv) the structural parameters show also nonlinear trends in this pressure range.[32] All these concurrent phenomena are the fingerprints of the amorphization and we suggest that some of them (if not all) can be related to the hybridization between bonding and nonbonding states and the consequent formation of a mixed phase.

ACKNOWLEDGMENTS

This work was supported by Grant No. 92-3-102-7 at Cineca (Casalecchio di Reno-Bologna-Italy). One of us (A.D.P.) gratefully acknowledges financial support from the "Fisica della Materia Condensata" Graduate School-Dipartimento di Fisica dell' Università de L'Aquila.

[1] H. D. Megaw, *Crystal Structure: A Working Approach* (Saunders, Philadelphia, 1973); R. Calas, P. Pascal, and J. Wyart, *Noveau Traité de Chimie Minérale* (Masson, Paris, 1965).

[2] E. Loh, Solid State Commun. **2**, 269 (1964).

[3] H. R. Philipp, Solid State Commun. **4**, 73 (1966); J. Phys. Chem. Solids **32**, 1935 (1971).

[4] T. H. DiStefano and D. E. Eastman, Solid State Commun. **9**, 2259 (1971).

[5] D. W. Fischer, J. Chem. Phys. **42**, 3814 (1965); G. Klein and H. U. Chun, Phys. Status Solidi B **49**, 167 (1972).

[6] G. Wiech, Solid State Commun. **52**, 807 (1984).

[7] T. H. DiStefano and D. E. Eastman, Phys. Rev. Lett. **27**, 1560 (1971).

[8] H. Ibach and J. E. Rowe, Phys. Rev. B **10**, 710 (1974); J. E. Rowe, Appl. Phys. Lett. **25**, 576 (1974).

[9] B. Fischer, R. A. Pollak, T. H. DiStefano, and W. D. Grobman, Phys. Rev. B **15**, 3193 (1977), and references therein.

[10] R. J. Hemley, A. P. Jephcoat, H. K. Mao, L. C. Ming, and M. H. Manghnani, Nature **334**, 52 (1988).

[11] R. M. Hazen, L. W. Finger, R. J. Hemley, and H. K. Mao, Solid State Commun. **72**, 507 (1989).

[12] R. R. Winters, A. Garg, and W. S. Hammack, Phys. Rev. Lett. **69**, 3751 (1992).

[13] O. Mishima, L. D. Calvert, and E. Whalley, Nature **310**, 393 (1984); G. C. Serghiou, R. R. Winters, and W. S. Hammack, Phys. Rev. Lett. **68**, 3311 (1992).

[14] M. B. Kruger and R. Jeanloz, Science **249**, 647 (1990).

[15] L. E. McNeil and M. Grimsditch, Phys. Rev. Lett. **68**, 83 (1992).

[16] K. L. Yip and W. B. Fowler, Phys. Rev. B **10**, 1400 (1974).

[17] S. T. Pantelides and W. A. Harrison, Phys. Rev. B **13**, 2667 (1976).

[18] R. B. Laughlin, J. D. Joannopoulos, and D. J. Chadi, Phys. Rev. B **20**, 5228 (1979).

[19] A. C. Lasaga and G. V. Gibbs, Phys. Chem. Miner. **14**, 107 (1987).

[20] S. Tsuneyuki, M. Tsukada, H. Aoki, and Y. Matsui, Phys. Rev. Lett. **61**, 869 (1988).

[21] A. C. Hess, P. F. McMillan, and M. O'Keeffe, J. Phys. Chem. **90**, 5661 (1986).

[22] S. Tsuneyuki, Y. Matsui, H. Aoki, and M. Tsukada, Nature **339**, 209 (1989).

[23] S. Tsuneyuki, H. Aoki, M. Tsukada, and Y. Matsui, Phys. Rev. Lett. **64**, 776 (1990); J. R. Chelikowsky, H. E. King, Jr., and J. Glinnemann, Phys. Rev. B **41**, 10866 (1990); J. S. Tse and D. D. Klug, Phys. Rev. Lett. **67**, 3559 (1991).

[24] M. S. Somayazulu, S. M. Sharma, N. Garg, S. L. Chaplot, and S. K. Sikka, J. Phys. Condens. Matter **5**, 6345 (1993).

[25] P. F. McMillan and A. C. Hess, Phys. Chem. Miner. **17**, 97 (1990).

[26] J. R. Chelikowsky and M. Schlüter, Phys. Rev. B **15**, 4020 (1977).

[27] R. Dovesi, C. Pisani, and C. Roetti, J. Chem. Phys. **86**, 6967 (1987); B. Silvi, P. D'Arco, and M. Causà, *ibid.* **93**, 7225 (1990); R. Nada, C. R. A. Catlow, R. Dovesi, and C. Pisani, Phys. Chem. Miner. **17**, 353 (1990).

[28] D. C. Allan and M. P. Teter, Phys. Rev. Lett. **59**, 1136 (1987).

[29] Y.-N. Xu and W. Y. Ching, Phys. Rev. B **44**, 11048 (1991), and references therein.

[30] K. T. Park, K. Terakura, and Y. Matsui, Nature **336**, 670 (1988).

[31] J. R. Chelikowsky, H. E. King, Jr., N. Troullier, J. L. Martins, and J. Glinnemann, Phys. Rev. Lett. **65**, 3309 (1990); J. R. Chelikowsky, N. Troullier, J. L. Martins, and H. E. King, Jr., Phys. Rev. B **44**, 489 (1991); N. Binggeli, N. Troullier, J. L. Martins, and J. R. Chelikowsky, *ibid.* **44**, 4771 (1991); N. Binggeli and J. R. Chelikowsky, Nature **353**, 344 (1991); Phys. Rev. Lett. **69**, 2220 (1992).

[32] A. Di Pomponio and A. Continenza, Phys. Rev. B **48**, 12558 (1993).

[33] H. Sowa, Z. Kristallogr. **184**, 257 (1988).

[34] L. Hedin and B. I. Lundqvist, J. Phys. C **4**, 2064 (1971).

[35] H. J. F. Jansen and A. J. Freeman, Phys. Rev. B **30**, 561 (1984).

[36] D. J. Chadi and M. L. Cohen, Phys. Rev. B **8**, 5747 (1973); H. J. Monkhorst and J. D. Pack, *ibid.* **13**, 5188 (1976).

[37] J. Rath and A. J. Freeman, Phys. Rev. B **11**, 2109 (1975).

[38] B. Welber, M. Cardona, C. K. Kim, and S. Rodriguez, Phys. Rev. B **12**, 5729 (1975); B. Welber, M. Cardona, Y. F. Tsay, and B. Bendow, *ibid.* **15**, 875 (1977); H. Müller, M. Cardona, and P. Vogl, *ibid.* **21**, 4879 (1980); S. Ves, K. Strössner, N. E. Christensen, C. K. Kim, and M. Cardona, Solid State Commun. **56**, 479 (1985).